J. Fluid Mech. (1993), *vol.* 253, *pp.* 593–615

Buckling of thin liquid jets

By B. TCHAVDAROV[1], A. L. YARIN[2] AND S. RADEV[1]

[1] Institute of Mechanics and Biomechanics, Bulgarian Academy of Sciences, Acad. G. Bonchev St., bl. No. 4, Sofia 1113, Bulgaria

[2] Faculty of Mechanical Engineering, Technion – Israel Institute of Technology, Haifa 32000, Israel

(Received 7 July 1992 and in revised form 22 January 1993)

The present work deals with the buckling phenomenon characteristic of highly viscous liquid jets slowly impinging upon a plate. The quasi-one-dimensional equations of the dynamics of thin liquid jets are used as the basis for the theoretical analysis of buckling. With the problem linearized, the characteristic equation is obtained. Its solutions show that instability (buckling) sets in only in the presence of axial compression in the jet, and when the distance between the nozzle exit and the plate exceeds some critical value. The latter is calculated. It is shown that buckling instability corresponds to the rectilinear jet/folding jet bifurcation point. The value of the folding frequency is calculated at the onset of buckling. The theoretical results are compared with Cruickshank & Munson's (1981) and Cruickshank's (1988) experimental data and the agreement is fairly good.

1. Introduction

Free liquid jets attract the attention of investigators in large measure because of their wide use in applications. Of no small importance is also that, due to the pioneering work of Rayleigh (1879), such flows became a classical example of hydrodynamic stability theory. In 1920–30 studies of free liquid jets were connected, first of all, with the development of engines, whereas in 1960–80 with ink-jet printers, jet rheometers, etc.

Beginning from the work of Rayleigh (1879) most attention has been paid to capillary jet breakup. In that case droplet separation results from the action of surface tension forces tending to minimize the free surface. Capillary breakup is characteristic only for low-velocity jets. The literature on linear and nonlinear effects in capillary breakup was reviewed by Bogy (1979) and Entov & Yarin (1984*b*) (see also the recent paper by Vassallo & Ashgriz 1991).

With an increase of the outflow velocity the dynamic action of the ambient gas has a growing effect on jet breakup (e.g. air). As a result of this, thin jets of liquids with low viscosity begin to atomize irregularly, whereas for jets of highly viscous liquids the type of instability leading to breakup is changed. The emerging new type of instability is related to the growth of bending disturbances under the dynamic action of air. This was studied by Weber (1931), Debye & Daen (1959) and Entov & Yarin (1984*a*) (see also the review of Entov & Yarin 1984*b*).

The experiments of G. I. Taylor (1969*a*, *b*) revealed a new type of instability in thin free jets and threads of highly viscous liquids moving at fairly low velocities and subject to longitudinal compression over a certain length. The longitudinal compressive force in these experiments originated either through friction between the jet and the air, or under longitudinal compression by a pair of rods, of a very viscous liquid thread lying

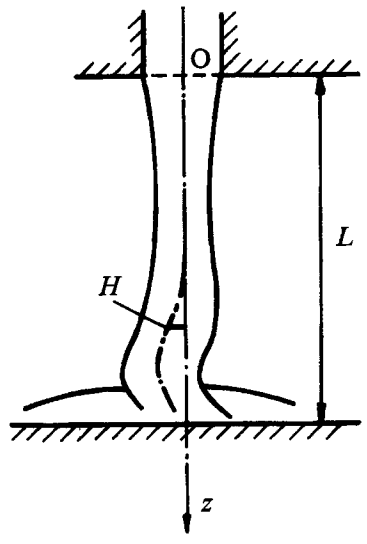

FIGURE 1. Buckling of a jet impinging upon a plate.

on the surface of mercury. Buckling was also observed in thin jets propagating in a liquid medium under the sudden increase in the density of the latter (and, consequently, in the buoyancy force) and when jets impinge normally onto a plate (see figure 1). Impinging jets of highly viscous liquids were studied in the experiments of Cruickshank & Munson (1981) and it was shown that buckling sets in at Reynolds numbers (under the conditions of jet issue) $Re < 1.2$. Jets with $Re > 1.2$ are stable and remain rectilinear on impingement. There is also a restriction on the distance L between the nozzle exit from which the jet issues and the plate. If L is less than a certain value L_1, there is no buckling. When $Re \leqslant 1.2$ and $L \geqslant L_1$, two-dimensional bending perturbations arise during which the jet axis remains a plane curve, and the jet piles up onto the plate in the form of folds. With increasing distance L, the bending perturbations acquire the form of a helix, the jet axis becomes three-dimensional, and the jet begins to coil at the plate in the form of rings. In Cruickshank & Munson's experiments buckling was also observed in highly viscous horizontal jets propagating along the free surface of a low-viscosity fluid (gravity excluded) when the jet begins to thicken immediately beyond the nozzle exit. Detailed reviews on liquid-jet buckling phenomena have been published by Entov & Yarin (1984*b*) and Bejan (1987).

The aim of the present paper is a theoretical description of the stability loss observed by Cruickshank & Munson (1981). The analysis is based on the quasi-one-dimensional equations of the dynamics of liquid jets derived by Entov & Yarin (1984*a*). A semi-empirical analysis of jet buckling was published by Cruickshank (1988), who introduced the additional assumption that the flow consists of two distinct regions: a far-field region in which the jet diameter is constant, and a near-plate region where the plate's effect is concentrated. Cruickshank also neglected gravity and surface tension when calculating critical buckling height. The present analysis dispenses with these assumptions.

The plan of the paper is as follows. In §2 the equations of the dynamics of thin liquid jets are briefly recovered. Then the system of governing equations is linearized in small buckling perturbations and reduced to an eigenvalue problem. In §§2–4 the analysis of the onset of buckling is first restricted to a simple model problem (without gravity and surface tension). The liquid thread is considered to be under a constant compressive

force between two fixed points. In spite of its restrictive character the simplified eigenvalue problem allows one a deeper insight in the nature of buckling instability of liquid jets. Under certain conditions its analytic solution is obtained in §3, whereas the numerical results are presented in §4. In §5 the real jet with gravity and surface tension is tackled. A numerical method for its solution is proposed in §6. The problem is treated in §7 where the results obtained are presented, discussed and compared with the experimental data In conclusion in §8 we summarize the results.

2. Governing equations and the model problem

The asymptotic system of quasi-one-dimensional equations of the dynamics of thin liquid jets has been derived by Entov & Yarin (1984*a*) from the integral balance equations of mass, momentum and moment of momentum. Solution of the problems of the hydrodynamics of free thin jets is reduced to the calculation of the distributions of such 'integral' parameters as the cross-sectional area A, the velocity of the liquid in the centre of gravity of the jet cross-section V, and the angular velocity of the liquid cross-section $\boldsymbol{\Omega}$, over the jet axis, and their evolution in time. The quasi-one-dimensional description holds under the assumption of jet slenderness, e.g. in the case when the scale length for variation along the jet is much greater than the radius of cross-section.

In the general case of spatial motion of a jet with circular cross-section the continuity, momentum and moment of momentum equations of the dynamics of free thin liquid jets read (Entov & Yarin 1984*a*)

$$\frac{\partial \lambda_1 A}{\partial t}+\frac{\partial WA}{\partial z}=0, \quad A=\pi a^2, \tag{2.1a}$$

$$\rho\left[\frac{\partial \lambda_1 AV}{\partial t}+\frac{\partial WAV}{\partial z}\right]=\frac{\partial}{\partial z}(F\boldsymbol{\tau}+\boldsymbol{Q})+\lambda_1 \rho \boldsymbol{g}A+\boldsymbol{q}\lambda_1, \tag{2.1b}$$

$$\boldsymbol{B}=\frac{\partial \boldsymbol{M}}{\partial z}+\lambda_1 \boldsymbol{\tau}\times\boldsymbol{Q}-\lambda_1 kI\boldsymbol{n}\times\rho\boldsymbol{g}+\lambda_1 \boldsymbol{m}. \tag{2.1c}$$

Here t is the time; z is an arbitrary parameter reckoned along the jet axis; W is the relative velocity of the liquid in the frame of reference associated with the jet; a is the radius of the jet cross-section; ρ is the density; $\boldsymbol{\tau}$ and $\boldsymbol{n}$ are the unit tangent vector and the unit principal-normal vector to the jet axis; $\boldsymbol{\tau}F$, $\boldsymbol{Q}$ and $\boldsymbol{M}$ represent the longitudinal force, the shearing force and the moment of stresses in the jet cross-section, respectively; $\boldsymbol{g}$ is the external force per unit mass, and $\boldsymbol{q}$ and $\boldsymbol{m}$ specify the linear density of external force and moment per unit length of the jet axis, respectively; $\boldsymbol{B}$ is the rate of change of the moment of momentum calculated by Entov & Yarin (1984*a*); $\lambda_1=|\partial \boldsymbol{R}/\partial z|$, where $\boldsymbol{R}(z,t)$ is the radius-vector of the jet axis; k is the curvature of the jet axis; $I=\frac{1}{4}\pi a^4$ is the moment of inertia of the jet cross-section. It should be noted that here we change the notation of Entov & Yarin (1984*a*) and use A instead of their f, z instead of s, F instead of P and $\boldsymbol{g}$ instead of $\boldsymbol{F}$.

Equation (2.1*a*) represents the mass balance inside an infinitesimally short element of the jet, and (2.1*b*) the balance of the forces applied to the element: inertial, internal and external. Equation (2.1*c*) represents the balance of the moments of these forces.

Equations (2.1) are closed by using the rheological constitutive equation of the liquid which allows one (accounting of the surface tension) to relate F and $\boldsymbol{M}$ with the kinematic parameters. In Entov & Yarin (1984*a*) this has been done for Newtonian liquid. Additionally some geometric and kinematic relations should be added to the

system (2.1). The most important of the kinematic relations is obtained under the condition that the jet surface is free from large shear stresses (such a relation will be used below in (2.8*a*)).

The system of equations (2.1) now is applied to the simplified model problem of highly viscous liquid jet buckling. As was shown in Cruickshank & Munson's (1981) experiments, the effect of inertia and surface tension of the liquid may be neglected at first approximation. First, we also, for simplicity study the case of a horizontal jet, for the moment excluding gravity from our considerations. The buckling of horizontal jets also was investigated by Cruickshank & Munson (1981), which gives relevance to the non-gravity case. Therefore, we may regard the buckling of the jet as plane when searching for the instability threshold. In the problem at hand we may neglect the aerodynamic forces acting on the jet, taking below $\boldsymbol{q} = \boldsymbol{0}$ and $\boldsymbol{m} = \boldsymbol{0}$. Under the assumptions made, the quasi-one-dimensional equations of continuity, momentum and moment of momentum of thin liquid jets (2.1) reduce to the following form (the perturbations being small):

$$\frac{\partial A}{\partial t}+\frac{\partial Aw}{\partial z}=0, \quad \frac{\partial F}{\partial z}=0, \quad Fk+\frac{\partial Q_n}{\partial z}=0, \tag{2.2a–c}$$

$$Q_n=-\frac{\partial}{\partial z}\left\{3\mu I\left[\frac{\partial}{\partial z}\left(\frac{\partial u}{\partial z}+kw\right)-\tfrac{1}{2}k\frac{\partial w}{\partial z}\right]\right\}, \quad F=3\mu A\frac{\partial w}{\partial z}. \tag{2.2d–e}$$

Here w and u are the projections of the liquid velocity in the jet on the tangent and normal to its axis, which is a plane curve; Q_n is the projection of the shearing force in the cross-section on the normal to the jet axis; μ is the viscosity of the liquid. The notation w and u is used instead of V_τ and V_n of Entov & Yarin (1984*a*), respectively.

Equation (2.2*a*) is that of continuity; (2.2*b*) and (2.2c) are the projections of the momentum equation of the tangent and normal to the axis of the jet; (2.2*d*) is the projection of the moment of momentum equation on the direction of the unit binormal vector to the axis of the jet, and (2.2*e*) results from the one-dimensional reduction of the rheological constitutive equation for a Newtonian fluid and connects the longitudinal force in the thin free jet with the rate of strain (3μ is the Trouton elongational viscosity).

Taking account of the fact that the following relationships hold for small perturbations (H is the amplitude of the plane deflection of the jet (see figure 1)):

$$u=\partial H/\partial t, \quad k=\partial^2 H/\partial z^2, \tag{2.3a, b}$$

we obtain, from (2.2*c–e*), the following equation, which is linear in the perturbations:

$$(a^0)^2\frac{\mathrm{d}w^0}{\mathrm{d}z}\frac{\partial^2 H}{\partial z^2}-\frac{1}{4L_*^2}\frac{\partial^2}{\partial z^2}\left[(a^0)^4\left(\frac{\partial^3 H}{\partial z^2\,\partial t}+w^0\frac{\partial^3 H}{\partial z^3}-\frac{1}{2}\frac{\mathrm{d}w^0}{\mathrm{d}z}\frac{\partial^2 H}{\partial z^2}\right)\right]=0. \tag{2.4}$$

In (2.4), $a^0(z)$ and $w^0(z)$ are the unperturbed distributions of the radius and velocity, which correspond to the rectilinear jet. Equation (2.4) is written in non-dimensional form; w_0^0 and L have been chosen as the scales for velocity and length, and a_0 (the subscript zero corresponds to the nozzle exit at $x = 0$) as the scale for the radius of the jet cross-section; $L_* = L/a_0$. Here, z is the coordinate along the unperturbed jet axis.

To determine $a^0(z)$ and $w^0(z)$, we use (2.2*a, b, e*) to obtain the following problem:

$$\frac{\mathrm{d}(a^0)^2w^0}{\mathrm{d}z}=0, \quad \frac{\mathrm{d}}{\mathrm{d}z}\left[(a^0)^2\frac{\mathrm{d}w^0}{\mathrm{d}z}\right]=0, \tag{2.5a, b}$$

$$z=0: \quad a^0=1, \quad w^0=1; \qquad z=1: \quad w^0=E. \tag{2.5c–e}$$

The boundary condition at the plate at $z = 1$ in (2.5) means in fact that the liquid flows through it at a velocity w_1^0 ($E = w_1^0/w_0^0$). Such a condition is needed in the absence of a solution of the stationary equations (2.5) which simultaneously satisfies the boundary conditions at the nozzle exit and the exact boundary condition $w^0 = 0$ at $z = 1$. The latter corresponds to an impermeable plate with an infinite spread of liquid over it. The condition at $z = 1$ in (2.5) enables us to model the slowing of the jet by the plate in the case $E < 1$ to a first approximation. Since at the surface of the plate, where the jet spreads, recourse to the quasi-one-dimensional equations is generally unjustified, there is no sense in constructing a more detailed unperturbed solution within this formulation. In the case of a perforated, partly permeable plate this condition, naturally, corresponds to reality.

Solutions to problem (2.5) were obtained by Matovich & Pearson (1969) in connection with fibre spinning (the case of $E > 1$), and have the form

$$w^0 = E^z, \quad (a^0)^2 = E^{-z}. \tag{2.6a, b}$$

In the jet-buckling problem under consideration here we obviously have $E < 1$. We can determine E in some specific situation by, say, comparing $a^0(z)$ from (2.6) with the experimentally observed profile of the jet near the point of stability loss (e.g. Cruickshank & Munson 1982). It should be stressed that the approximations (2.6) suffice for a qualitative analysis of the causes of stability loss, since under them the longitudinal force F divided by $3\mu\pi a_0^2 w_0^0/L$ equals $\ln E$ by (2.2*e*): the case $E > 1$ relates to a tensile force $F > 0$ (fibres), and $E < 1$ to a compressive force, $F < 0$.

In spite of the fact that in our simplified model the condition of the plate impermeability is discarded, the liquid approaching the plate is decelerated (the plate resists the liquid flow through it when $w_1^0 < w_0^0$, $E < 1$). As a result, the internal viscous stresses in the jet cross-section are compressive and the jet is under a constant compressive force as a whole.†

A more realistic unperturbed solution for $a^0(z)$ and $w^0(z)$ may be obtained by inclusion of the gravity force (if any) along the jet axis. Such a solution was found by Cruickshank & Munson (1982). Inclusion of the gravity force enabled them to use $w^0 = 0$ at $z = 1$ as boundary condition at the plate surface. This solution, as well as its stability, will be considered later in the present work. However, we first investigate the stability of the model solution (2.6).

Assuming $H(z, t) = \exp(\lambda t) f(z)$ (λ is the eigenvalue, $f(z)$ the eigenfunction), we obtain by means of (2.4) and (2.6) the characteristic equation

$$\frac{\mathrm{d}^2}{\mathrm{d}z^2}\left\{f \ln E - \frac{1}{4L_*^2}\left[E^{-2z}\left(\lambda \frac{\mathrm{d}^2 f}{\mathrm{d}z^2} + E^z \frac{\mathrm{d}^3 f}{\mathrm{d}z^3} - \frac{E^z \ln E}{2} \frac{\mathrm{d}^2 f}{\mathrm{d}z^2}\right)\right]\right\} = 0. \tag{2.7}$$

To solve the problem we need, generally speaking, to consider the edge regions of the jet near the nozzle exit and near the plate. In these regions the quasi-one-dimensional equations are inapplicable and Navier–Stokes equations have to be solved satisfying the boundary conditions at the nozzle exit, the no-slip condition at the plate surface and the conditions for the internal stresses at the free surface. The solutions of the Navier–Stokes equations must match that of (2.7). The difficulties involved in using the

† It should be noted that the steady-state viscosity-dominated jet configuration in the buckling problems has nothing in common with that of planar irrotational inviscid jet flows incident on impermeable or semi-impermeable (porous) walls, which have been studied by using the hodograph method or some other transformations (see Birkhoff & Zarantonello 1957; Gurevich 1965, Jenkins & Barton 1988; King 1990).

Navier–Stokes equations can be overcome by staying within the bounds of the quasi-one-dimensional theory. Indeed, two of the five conditions needed for (2.7) are obvious: (*a*) absence of any displacement of the jet axis at $z = 0$; (*b*) a smooth junction of the tangent to the jet axis and the nozzle at $z = 0$.

The three remaining conditions can be found from Entov & Yarin's (1984*a*) expressions for the angular velocity of the liquid cross-section $\boldsymbol{\Omega}$, and the moment of stresses in the jet cross-section $\boldsymbol{M}$ which in our case are

$$\Omega_b = \frac{\partial u}{\partial z} + kw^0, \quad M_b = 3\mu \frac{\pi(a^0)^4}{4}\left[\frac{\partial^2 u}{\partial z^2} + w^0 \frac{\partial k}{\partial z} - \frac{k}{2}\frac{\mathrm{d}w^0}{\mathrm{d}z}\right]. \tag{2.8a, b}$$

The relations (2.8) are written in dimensional form for small bending perturbations; for plane buckling only the projections of $\boldsymbol{\Omega}$ and $\boldsymbol{M}$ onto the binormal to the jet axis need be considered.

In addition to the two boundary conditions already formulated, we consider four types of additional conditions and their relevance from the physical point of view.

(i) The moment of internal stresses vanishes ($M_b = 0$) at $z = 0$ and $z = 1$.

(ii) There is no rotation of the liquid cross-section at the nozzle exit, which means $\Omega_b = 0$ at $z = 0$ (during buckling of the jet an angular velocity generally appears, directed along the binormal to the axis, $\Omega_b \neq 0$), and $M_b = 0$ at the plate ($z = 1$).

(iii) At $z = 0$, $M_b = 0$ and the jet axis is clamped at $z = 1$.

(iv) At $z = 0$, $\Omega_b = 0$ and the jet axis is clamped at $z = 1$.

We also assume throughout that there is no displacement of the jet axis at $z = 1$. Thus, allowing for (2.8), we shall seek a solution to (2.7) with the following boundary conditions:

$$z = 0: \quad f = 0, \quad \frac{\mathrm{d}f}{\mathrm{d}z} = 0, \quad \lambda\frac{\mathrm{d}^2 f}{\mathrm{d}z^2} + E^z\frac{\mathrm{d}^3 f}{\mathrm{d}z^3} - \frac{E^z \ln E}{2}\frac{\mathrm{d}^2 f}{\mathrm{d}z^2} = 0; \tag{2.9a–c}$$

$$z = 1: \quad f = 0, \quad \lambda\frac{\mathrm{d}^2 f}{\mathrm{d}z^2} + E^z\frac{\mathrm{d}^3 f}{\mathrm{d}z^3} - \frac{E^z \ln E}{2}\frac{\mathrm{d}^2 f}{\mathrm{d}z^2} = 0, \tag{2.9d, e}$$

or

$$z = 0: \quad f = 0, \quad \mathrm{d}f/\mathrm{d}z = 0, \quad \mathrm{d}^2 f/\mathrm{d}z^2 = 0; \tag{2.10a–c}$$

$$z = 1; \quad f = 0, \quad \lambda\frac{\mathrm{d}^2 f}{\mathrm{d}z^2} + E^z\frac{\mathrm{d}^3 f}{\mathrm{d}z^3} - \frac{E^z \ln E}{2}\frac{\mathrm{d}^2 f}{\mathrm{d}z^2} = 0, \tag{2.10d, e}$$

or

$$z = 0: \quad f = 0, \quad \frac{\mathrm{d}f}{\mathrm{d}z} = 0, \quad \lambda\frac{\mathrm{d}^2 f}{\mathrm{d}z^2} + E^z\frac{\mathrm{d}^3 f}{\mathrm{d}z^3} - \frac{E^z \ln E}{2}\frac{\mathrm{d}^2 f}{\mathrm{d}z^2} = 0; \tag{2.11a–c}$$

$$z = 1: \quad f = 0, \quad \mathrm{d}f/\mathrm{d}z = 0, \tag{2.11d, e}$$

or

$$z = 0: \quad f = 0, \quad \mathrm{d}f/\mathrm{d}z = 0, \quad \mathrm{d}^2 f/\mathrm{d}z^2 = 0; \tag{2.12a–c}$$

$$z = 1: \quad f = 0, \quad \mathrm{d}f/\mathrm{d}z = 0. \tag{2.12d, e}$$

For each of these four sets of the boundary conditions we will obtain buckling (similarly to the theory of elastic beams). However, in the case of liquid jets some of them correspond to rather artificial situations, namely the conditions $M_b = 0$ at $z = 0$ and $z = 1$. The jet corresponding to such conditions might exist when the nozzle and plate are heated, and the viscosity of the liquid in contact with them is low. However, the thin jet is cooled rapidly by the ambient gas and the liquid viscosity increases steeply. Under these circumstances we obtain from (2.8*b*) $M_b = 0$ at $z = 0$

and $z = 1$, and M_b is not zero inside a jet. Although such a situation seems rather artificial, it deserves consideration, as it permits analytical treatment (see below) and sheds light on some general trends in stability loss.

In an isothermal situation a 'clamp' on the jet axis at the plate looks like the most appropriate condition from the physical point of view because the jet spreads at the plate, its radius and the moment of inertia becoming comparatively large. Therefore, according to (2.8*b*), the moment of internal stresses in cross-sections near the plate should be also very large. As a result the jet strongly resists rotation of its material cross-section by a compressive force, which corresponds to the 'clamp' condition.

The condition $\Omega_b = 0$ at the nozzle exit $z = 0$ is the most appropriate one, since the liquid cross-section cannot immediately acquire rotation (as a result of the inertia), which is absent at $z = -0$ inside a nozzle. Thereby, it is natural to expect that the jets of Cruickshank & Munson's (1981) and Cruickshank's (1988) experiments correspond to the boundary conditions (2.12).

Nevertheless, first we consider the simplified artificial situation that allows an analytical solution to be obtained.

3. Analytic asymptotic solution

We investigate first the problem (2.7), (2.9), assuming that $\lambda = 0$, i.e. investigate the possibility of aperiodic loss of stability. Integrating twice, we obtain from (2.7) with the aid of (2.9)

$$\frac{\mathrm{d}^3 f}{\mathrm{d}z^3} - \frac{\ln E}{2}\frac{\mathrm{d}^2 f}{\mathrm{d}z^2} - (4L_*^2 E^z \ln E) f = 0. \tag{3.1}$$

Now consider the case when

$$E = 1 + \zeta, \quad |\zeta| \ll 1. \tag{3.2a,b}$$

Substituting (3.2) in (3.1) and disregarding small terms of higher orders in ζ, we obtain a linear differential equation with constant coefficients

$$\frac{\mathrm{d}^3 f}{\mathrm{d}z^3} - \frac{\zeta}{2}\frac{\mathrm{d}^2 f}{\mathrm{d}z^2} - 4L_*^2 \zeta f = 0. \tag{3.3}$$

On searching for its particular solutions in the form $f = \text{const} \times \exp(mz)$, we arrive at the cubic equation

$$m^3 - \zeta \tfrac{1}{2} m^2 - 4L_*^2 \zeta = 0. \tag{3.4}$$

Using Cardan's solution and again disregarding small terms of higher orders in ζ, we obtain solution to (3.4) in the form

$$m_1 = U, \quad m_2 = U(-\tfrac{1}{2} - \mathrm{i}\tfrac{1}{2}\sqrt{3}), \quad m_3 = U(-\tfrac{1}{2} + \mathrm{i}\tfrac{1}{2}\sqrt{3}), \quad U = (4L_*^2 \zeta)^{\frac{1}{3}}. \tag{3.5a–d}$$

The general solution to the differential equation (3.3) allowing for (3.5) acquires the form

$$f(z) = C_1 \exp(Uz) + \exp(-\tfrac{1}{2}Uz)[C_2 \cos(\tfrac{1}{2}\sqrt{3}\,Uz) + C_3 \sin(\tfrac{1}{2}\sqrt{3}\,Uz)]. \tag{3.6}$$

To determine the constants C_i, we use the three remaining boundary conditions in (2.9*a*, *b*, *d*). Consequently, we find with the aid of (3.6) the condition for non-triviality of the solution to the linear system obtained of three equations in C_1, C_2 and C_3:

$$\exp(\tfrac{3}{2}U) = \sqrt{3}\sin(\tfrac{1}{2}\sqrt{3}\,U) + \cos(\tfrac{1}{2}\sqrt{3}\,U). \tag{3.7}$$

The left- and right-hand sides of (3.7) are shown as functions of U in figure 2.

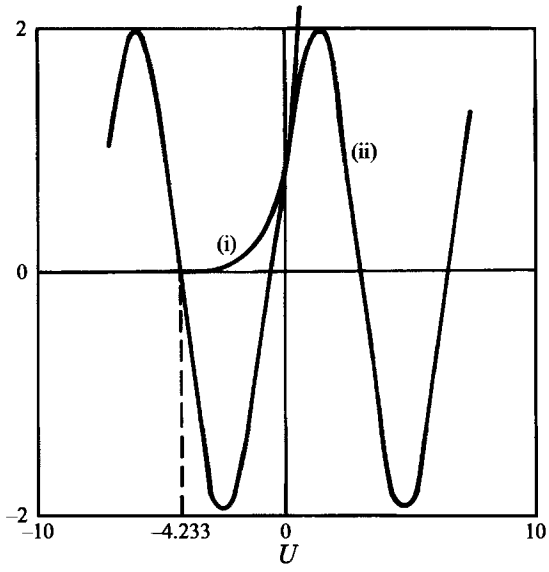

FIGURE 2. Left-hand (curve i) and right-hand (curve ii) sides of (3.7).

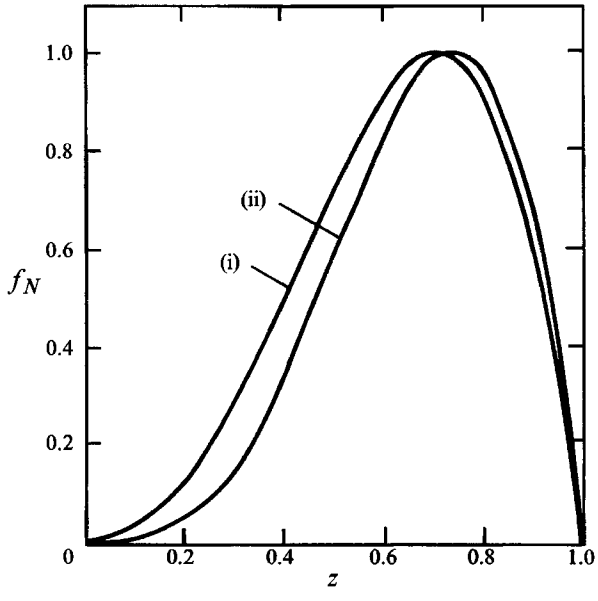

FIGURE 3. Eigenfunctions corresponding to boundary conditions (2.9) (curve i) and (2.10) (curve ii).

Clearly, when $U > 0$, (3.7) cannot be satisfied. By the expression for U in (3.5), this means that there cannot possibly be any non-trivial positions of 'equilibrium' (with a curved axis) in the case of stretching of the jet ($E > 1$, $\zeta > 0$; fibre). The solution $U = 0$ to (3.7), with allowance for (3.6) and (2.9), yields the trivial eigenfunction $f \equiv 0$. By contrast, in the case of compression of the jet as it impinges upon a plate, when $E < 1$, $\zeta < 0$, and $U < 0$, there are solutions to (3.7) which lead to non-trivial eigenfunctions. Consequently, there are in this case non-trivial forms of 'equilibrium' of the jet axis (with deflection), and aperiodic loss of stability takes place (when $\lambda = 0$). The required solution $U = U_* < 0$ to (3.7) corresponds to the root of least modulus, since

instability sets in at the shortest of all possible distances between the nozzle and the plate. Accordingly, we obtain from (3.7) $U = U_* = -4.233$; the eigenfunction corresponding to this value of U has the form

$$f(z)/C_1 = \exp(U_* z) - \exp(-\tfrac{1}{2}U_* z)[\cos(\tfrac{1}{2}\sqrt{3}\,U_* z) + \sqrt{3}\sin(\tfrac{1}{2}\sqrt{3}\,U_* z)] \quad (3.8)$$

and is shown in figure 3, curve (i) ($f_N = f/f_{\max}$).

We use (3.2*a*) and (3.5*d*) to find the quantity L_* corresponding the aperiodic loss of stability:

$$L_{*1} = \frac{L_1}{a_0} = \left(\frac{U_*^3}{4(E-1)}\right)^{\frac{1}{2}} = \frac{4.355}{(1-E)^{\frac{1}{2}}}. \quad (3.9)$$

If with the given value of E, dictated by the conditions of the experiment, the distance between the nozzle and the plate exceeds the value predicted by (3.9), then at least aperiodic loss of stability will take place–buckling of the liquid jet or thread. The problem of the presence of other forms of stability loss when λ is a complex number with a positive real part is solved below by numerical analysis.

4. Numerical solution of the model problem

First we consider the results of numerical solution of (2.7) with boundary conditions (2.10) corresponding to $0 < E < 1$ (for the method of solution see §6). Unlike the preceding asymptotical analysis, E is now not always close to unity. Figure 4 shows the real and imaginary parts (λ_r and λ_i) of the first eigenvalue λ as function of L_* for certain values of E. It is clear that for L_* less than a certain critical value L_{*1}, the real part satisfies $\lambda_r < 0$ and the jet is stable. On the other hand, when $L_* > L_{*1}$ the real part satisfies $\lambda_r > 0$, $\lambda_i \equiv 0$ and the jet is unstable – buckling takes place. The critical value L_{*1} for an arbitrary fixed E is defined by the eigenvalue whose real part first attains zero with an increase in L_*. This corresponds to the point of stability loss determined in the experiment during a gradual increase in the distance between the nozzle and the plate.

Thus, the numerical solution of (2.7) and (2.10) shows, in accordance with the results of the preceding asymptotical analysis, that stability is lost when there is an increase in the distance between the nozzle and the plate up to the value $L_1 = L_{*1}a_0$. The dependence of L_{*1} on $1/E(\sim w_0^0)$, which illustrates the change in the critical length at which stability is lost with increase in the rate of outflow of the jet from the nozzle, is shown in figure 5, curve (i). The eigenfunction obtained in the calculation with $E = 0.8$, $L_* = L_{*1} = 13.8$, is shown in figure 3, curve (ii) ($f_N = f/f_{\max}$).

A numerical solution was also found for (2.7) and (2.9), which was studied analytically in §3 for values of E close to unity. The dependence of L_{*1} on $1/E$ obtained numerically in this case is shown in figure 5, curve (ii). In the same figure curve (iii), which practically merges with curve (ii) as E approaches unity, represents the asymptotic result (3.9). Comparison with the numerical solution shows that the accuracy of (3.9) is fairly high even when $E = 0.1$, i.e. far beyond the limit of applicability of the asymptotic form. The eigenfunction determined in the numerical solution of (2.7) and (2.9) for $E = 0.8$, $L_* = L_{*1} = 9.74$ and divided by the value at the maximum practically coincides with curve (i) in figure 3. This shows yet again that the asymptotic solution (3.8) gives a satisfactory degree of accuracy not only as $E \to 1$, but also at values of E appreciably less than unity.

As in the numerical solution of the problem (2.6) and (2.10), the eigenvalue $\lambda = 0$ corresponds to loss of stability when $L_* = L_{*1}$ for arbitrary values $0 < E < 1$.

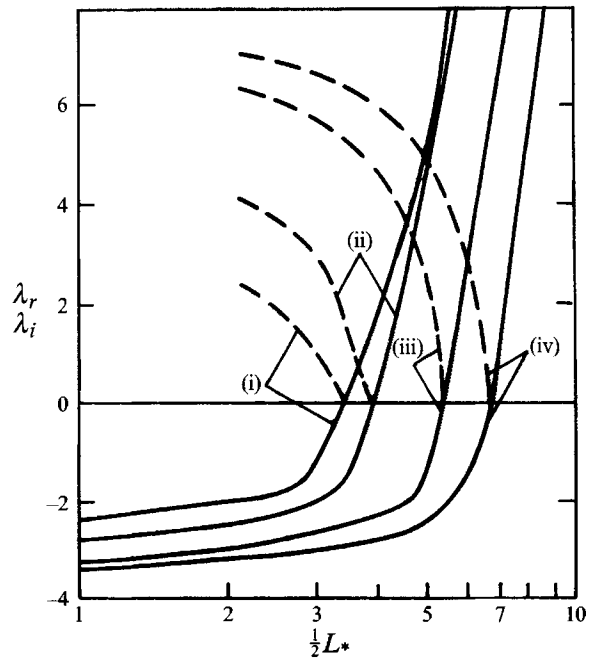

FIGURE 4. Real and imaginary parts of eigenvalue λ of (2.7) under boundary conditions (2.10). solid curves represent λ_r, dashed ones λ_i. Curves (i) correspond to $E = 0.2$, (ii) 0.4, (iii) 0.7, (iv) 0.8.

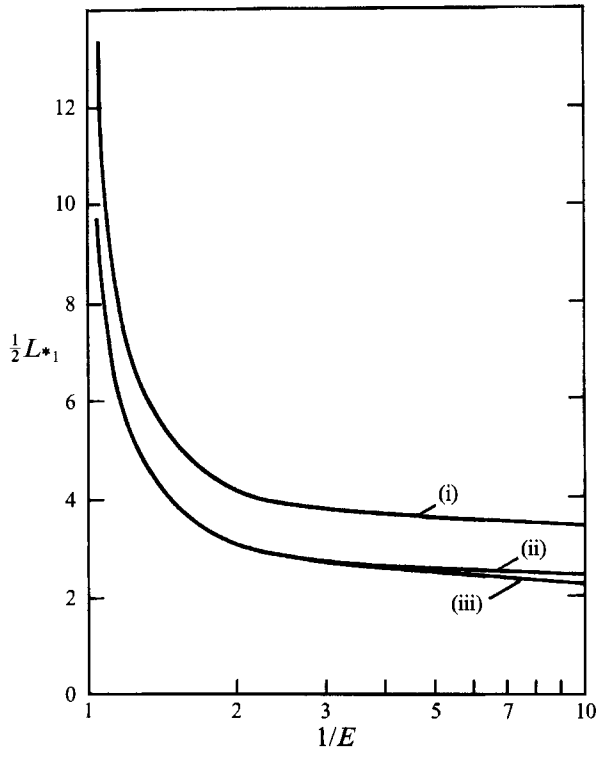

FIGURE 5. Dependence of critical distance to plate on outflow rate: Curve (i) corresponds to problem (2.7) under boundary conditions (2.10); curve (ii) to (2.7) under boundary conditions (2.9); curve (iii) to asymptotic result (3.9) for (2.7), (2.9).

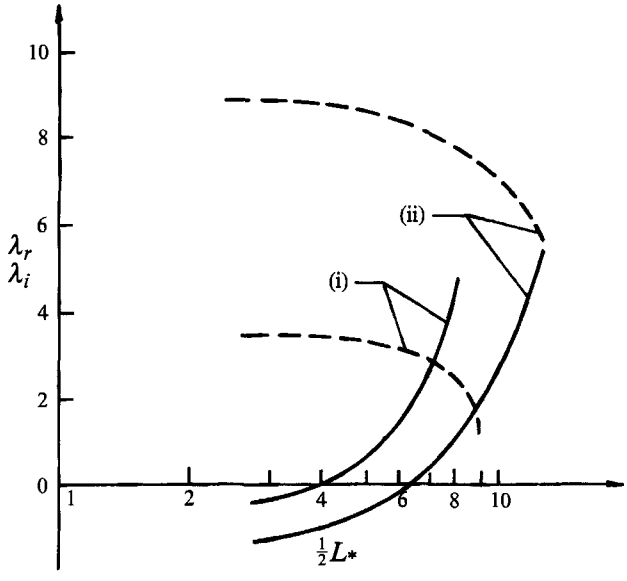

FIGURE 6. First eigenvalue of (2.7), (2.12) under the 'clamp' boundary condition. Solid curves represent λ_r, dashed ones λ_i. Curves (i) correspond to $E = 0.2$, (ii) to 0.8.

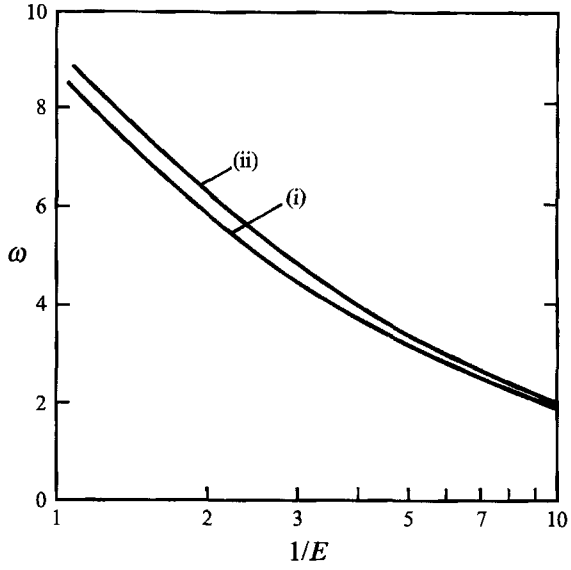

FIGURE 7. Folding frequency: curve (i) eigenvalue problem (2.7), (2.11); (ii) (2.7), (2.12).

Let us now consider the numerical results for two eigenvalue problems with 'clamp' conditions: (2.7), (2.11) and (2.7), (2.12). The first eigenvalue of the second problem is plotted in figure 6. In contrast with figure 4, at a critical length $L_* = L_{*1}$ the imaginary part of the first eigenvalue $\lambda_i > 0$, i.e. stability loss is accompanied by onset of self-sustained oscillations (folding) as observed experimentally. The same conclusion applied for problem (2.7), (2.11). Therefore, the 'clamp' boundary condition in (2.11) and (2.12) yields folding at the point of stability loss. The folding frequency $\omega = \lambda_i$ corresponding to the critical (buckling) height is shown in figure 7. The buckling height under the 'clamp' conditions (2.11) and (2.12) is plotted in figure 8.

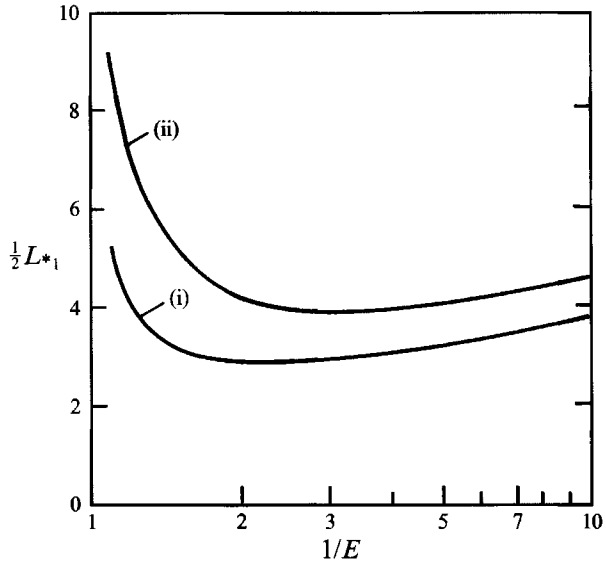

FIGURE 8. Buckling height: Curve (i) corresponds to (2.7), (2.11), (ii) to (2.7), (2.12).

The results presented in figures 6–8 support the conclusions drawn in §2 that the 'clamp' condition at $z = 1$ is the most appropriate one from the physical point of view.

Let us now consider the reasons for the existence of a critical distance L_{*1} between the nozzle exit and the plate, below which the jet or thread is stable. In accordance with (2.2*c–e*) and (2.4), the balance of the following force moments corresponds to motion of a liquid in a jet:

$$M_1 = 3\mu A^0 \frac{dw^0}{dz} H, \quad M_2 = -3\mu I^0 \left(w^0 \frac{\partial k}{\partial z} - \tfrac{1}{2} k \frac{dw^0}{dz} \right), \quad M_3 = -3\mu I^0 \frac{\partial^3 H}{\partial z^2 \, \partial t}. \tag{4.1a–c}$$

All relationships here are written in dimensional form for small bending perturbations; M_1 is the bending moment due to longitudinal compression; M_2 and M_3 are the moments of the viscous stresses due to motion of a liquid particle along a curved trajectory and to curvature change with time. As the distance between the nozzle exit and the plate decreases, the moment M_2 increases sharply, since its magnitude is determined by the leading derivative $\partial k/\partial z = \partial^3 H/\partial z^3$. Consequently, for sufficiently small distances L, M_1 cannot overcome M_2 and the flow is stable. M_1 begins to dominate only for $L > L_1$.

5. Inclusion of gravity and surface tension

In vertical jets and threads, the effect of gravity and surface tension has to be taken into account, both in an unperturbed solution and in a linear stability problem. In the case considered here using Entov & Yarin's (1984*a*) equations of thin jet dynamics (see also (2.1)) we obtain instead of (2.2*b–e*) the following system:

$$\frac{1}{\rho}\frac{\partial F}{\partial z} + Ag = 0, \quad \frac{1}{\rho}\left(Fk + \frac{\partial Q_n}{\partial z} \right) - Ag \frac{\partial H}{\partial z} = 0, \quad \frac{1}{\rho}\left(\frac{\partial M_b}{\partial z} + Q_n \right) + k\,Ig = 0, \tag{5.1a–c}$$

where
$$F = 3\mu\frac{\partial w}{\partial z}A + \gamma\pi\left\{\frac{a}{(1+(\partial a/\partial z)^2)^{\frac{1}{2}}} + \frac{a^2\,\partial^2 a/\partial z^2}{[1+(\partial a/\partial z)^2]^{\frac{3}{2}}}\right\}, \tag{5.2a}$$

$$M_b = 3\mu I\left(\frac{\partial \Omega_b}{\partial z} - \tfrac{3}{2}k\frac{\partial w}{\partial z}\right) - \frac{\gamma k I}{a[1+(\partial a/\partial z)^2]^{\frac{3}{2}}}, \quad \Omega_b = \frac{\partial u}{\partial z} + kw, \tag{5.2b,c}$$

and g is gravity acceleration, γ is surface tension. Note that Entov & Yarin (1984*a*) used the notation α for surface tension.

Equation (2.2*a*) remains valid alongside (5.1) and (5.2) without any change.

Linearizing the problem thus obtained, and bearing in mind (2.3), we find the following equation for the eigenfunction f corresponding to the displacement amplitude $H = f(z)\exp(\lambda t)$:

$$\frac{2}{a^0}\frac{\mathrm{d}a^0}{\mathrm{d}z}\frac{\mathrm{d}^2 f}{\mathrm{d}z^2} - \frac{\delta}{3}\left\{\frac{a^0}{[L_*^2+(\mathrm{d}a^0/\mathrm{d}z)^2]^{\frac{1}{2}}} + \frac{a^{02}\,\mathrm{d}^2 a^0/\mathrm{d}z^2}{[L_*^2+(\mathrm{d}a^0/\mathrm{d}z)^2]^{\frac{3}{2}}}\right\}\frac{\mathrm{d}^2 f}{\mathrm{d}z^2}$$
$$+\frac{1}{4L_*^2}\frac{\mathrm{d}^2}{\mathrm{d}z^2}\left\{a^{04}\left[\lambda\frac{\mathrm{d}^2 f}{\mathrm{d}z^2} + \frac{1}{a^{02}}\frac{\mathrm{d}^3 f}{\mathrm{d}z^3} + \frac{1}{a^{03}}\frac{\mathrm{d}a^0}{\mathrm{d}z}\frac{\mathrm{d}^2 f}{\mathrm{d}z^2}\right.\right.$$
$$\left.\left. - \frac{\delta}{3a^0}\frac{L_*^2\,\mathrm{d}^2 f/\mathrm{d}z^2}{[L_*^2+(\mathrm{d}a^0/\mathrm{d}z)^2]^{\frac{3}{2}}}\right]\right\} + 2GL_*^2\left[\frac{1}{4L_*^2}\frac{\mathrm{d}}{\mathrm{d}z}\left(a^{04}\frac{\mathrm{d}^2 f}{\mathrm{d}z^2}\right) + a^{02}\frac{\mathrm{d}f}{\mathrm{d}z}\right] = 0, \tag{5.3}$$

with the non-dimensional parameters

$$G = \rho g a_0^2/6\mu w_0^0, \quad \delta = \gamma L^2/\mu w_0^0 a_0^2 \tag{5.4a,b}$$

representing the ratios of the gravity and surface forces to their viscous counterparts. With $G = \delta = 0$ and $a^0 = E^{-z/2}$, (5.3) reduces to (2.7).

At the nozzle exit the boundary conditions of the absence of jet displacement, smooth junction of the jet axis with the nozzle, and zero angular velocity of the liquid cross-section are posed. At the other end of the jet it is assumed that the jet axis is 'clamped' at the wall. Thus, (5.3) is solved under boundary conditions (2.12), which seem the most realistic as follows from the discussion in §2.

To solve the above eigenvalue problem, a solution for a steady-state jet radius $a^0(z)$ is needed. With the longitudinal force taken as $F = 3\mu A\,\partial w/\partial z + \gamma\pi a$, which simplifies (5.2*a*), the continuity and longitudinal momentum equations (2.2*a*) and (5.1*a*)) reduce to

$$a^0\frac{\mathrm{d}^2 a^0}{\mathrm{d}z^2} - \left(\frac{\mathrm{d}a^0}{\mathrm{d}z}\right)^2 = \beta^2 a^{04} + \frac{1}{6L_*}\delta\frac{\mathrm{d}a^0}{\mathrm{d}z}a^{02}, \quad \beta^2 = L_*^2 G, \tag{5.5a,b}$$

As an unperturbed jet approaches the plate surface normally, the velocity w^0 tends to zero because of the impermeability of the wall, and the jet radius tends to infinity. Thus, the boundary conditions to be applied for (5.5) are as follows:

$$z = 0: \quad a^0 = 1; \quad z = 1: \quad a^0 = \infty. \tag{5.6a,b}$$

Analyzing the data of Cruickshank & Munson (1981) and Cruickshank (1988) we observe that in their experiments the ratio $\delta/6L_*$ is much smaller (or significantly smaller) than β^2 (the estimates are given below in §7). Under such conditions numerical calculations show that the solution of (5.5), (5.6) is all but insensitive to the last term in (5.5*a*) with the surface tension parameter δ. Therefore, it is justified to take $\delta = 0$ and obtain, instead of (5.5), the following equation which has an analytical solution:

$$a^0\frac{\mathrm{d}^2 a^0}{\mathrm{d}z^2} - \left(\frac{\mathrm{d}a^0}{\mathrm{d}z}\right)^2 = \beta^2 a^{04}. \tag{5.7}$$

The solution of (5.7), (5.6) was obtained by Cruickshank & Munson (1982) and reads

$$a^0(z) = \frac{\sinh(D\beta)}{\sinh[D\beta(1-z)]}, \quad 0 < \beta < 1 \tag{5.8}$$

$$a^0(z) = \frac{1}{1-z}, \quad \beta = 1, \tag{5.9}$$

$$a^0(z) = \frac{\sin(D_1\beta)}{\sin[D_1\beta(1-z)]}, \quad \beta > 1. \tag{5.10}$$

In (5.8) D is a positive solution of the equation

$$D = \sinh(D\beta), \tag{5.11}$$

whereas in (5.10) D_1 is a solution of

$$D_1 = \sin(D_1\beta), \tag{5.12}$$

where D_1 belongs to the interval $(0, \pi/\beta)$.

If $\beta < \frac{1}{2}\pi$ the jet is in compression from the very beginning and $\mathrm{d}a^0/\mathrm{d}z > 0$. In this case the effect of liquid deceleration by the plate and emerging compressive viscous force is stronger than the effect of gravity acceleration. In a sense the dependence $a^0(z)$ for $\beta < \frac{1}{2}\pi$ is qualitatively similar to that of the model problem considered in §2, (2.6).

If $\beta > \frac{1}{2}\pi$ the jet is in tension from the nozzle exit up to some cross-section ($\mathrm{d}a^0/dz < 0$) (gravity acceleration dominates) but the last portion of the jet near the plate is in compression and $\mathrm{d}a^0/\mathrm{d}z > 0$ (the viscous compressive force dominates). This case is completely distinct from the model problem of §2.

The behaviour of liquid jet in microgravity under the action of viscous forces and surface tension might be studied by using the solution of (5.5), (5.6) with $\beta = 0$. This solution reads

$$a^0(z) = \frac{P}{(\delta/6L_*)\{\exp[P(1-z)]-1\}} \tag{5.13}$$

for $\delta/6L_*$ not unity, and

$$a^0(z) = 1/(1-z), \quad \delta/6L_* = 1. \tag{5.14a, b}$$

In (5.13) for $0 < \delta/6L_* < 1$ P is a positive solution of the equation

$$P = \ln\left(\frac{\delta/6L_* + P}{\delta/6L_*}\right), \tag{5.15}$$

whereas for $\delta/6L_* > 1$ P is a solution of (5.15) belonging to the interval $(-\delta/6L_*, 0)$.

According to (5.13)–(5.15) the longitudinal force F divided by $6\mu\pi a_0^2 w_0^0/L$ equals $-P$: the case $\delta/6L_* > 1$ when $P < 0$ relates to a tensile force $F > 0$, and $\delta/6L_* < 1$ to a compressive force, $F < 0$. Hence, the solution (5.13)–(5.15) is expected to be unstable only for $\delta/6L_* < 1$ when it is qualitatively similar to the solution of the model problem of §2.

6. Numerical method of solution

Using the substitutions

$$y_k = (1-z)^{k-1}\Phi^{(k)}(z) \quad (k = 0, 1, 2, 3, 4), \qquad Y = (y_0, y_1, y_2, y_3, y_4)^{\mathrm{T}} \tag{6.1}$$

the problem (5.3), (2.12) is transformed into an eigenvalue problem for a system of first-order linear differential equations

$$(1-z)^2\, Y'(z) + A(z;\lambda)\, Y(z) = 0, \quad z \in [0, 1], \tag{6.2}$$

$$\Psi_0^{\mathrm{T}}\, Y = 0, \quad z = 0; \qquad \Psi_1^{\mathrm{T}}\, Y = 0, \quad z = 1, \tag{6.3a, b}$$

where $\boldsymbol{A}(z;\lambda)$ is a 5×5 matrix of continuous components about $z\in[0,1]$ and depending on λ; $\boldsymbol{\Psi}_0^{\mathrm{T}}$ and $\boldsymbol{\Psi}_1^{\mathrm{T}}$ are scalar matrices of order 5×3 and 5×2, respectively ($\boldsymbol{\Psi}^{\mathrm{T}}$ denoting the transpose of $\boldsymbol{\Psi}$).

The problem (6.2), (6.3) is a singular eigenvalue problem (the singularity being due to $a^0(z)\to\infty$ as $z\to 1$). To solve it, we use the method proposed by Abramov (1961). Let $\boldsymbol{Y}(z;\lambda)$ be an arbitrary solution of the system (6.2) satisfying the boundary condition at $z=1$. Then, as has been proved by Abramov (1961), the solution $\boldsymbol{\Psi}(z;\lambda)$ of the initial value problem

$$\boldsymbol{\Psi}'-(\boldsymbol{B}^{\mathrm{T}}-\boldsymbol{\Psi}(\boldsymbol{\Psi}^{\mathrm{T}}\boldsymbol{\Psi})^{-1}\boldsymbol{\Psi}^{\mathrm{T}}\boldsymbol{B}^{\mathrm{T}})\boldsymbol{\Psi}=\boldsymbol{0},\quad \boldsymbol{B}=\boldsymbol{A}(1-z)^{-2},\quad z\in[0,1],\qquad (6.4a,b)$$

$$\boldsymbol{\Psi}=\boldsymbol{\Psi}_1,\quad z=1 \qquad (6.5)$$

satisfies

$$\boldsymbol{\Psi}(z;\lambda)\,\boldsymbol{Y}(z;\lambda)=\boldsymbol{0}\quad\text{for any}\quad z\in[0,1], \qquad (6.6)$$

i.e. the boundary conditions at $z=1$ can be shifted to any $z\in[0,1]$.

Hence, integrating (6.4), (6.5) up to $z=0$, the required eigenvalue relation is obtained in the form

$$\det\begin{pmatrix}\boldsymbol{\Psi}_0^{\mathrm{T}}\\ \boldsymbol{\Psi}_{1,0}^{\mathrm{T}}(\lambda)\end{pmatrix}=0, \qquad (6.7)$$

where $\boldsymbol{\Psi}_{1,0}(\lambda)$ denotes the solution of (6.4), (6.5) at $z=0$.

Using the bi-directional strategy, i.e. integrating (6.4) from both sides of the interval up to a prescribed interior point, the characteristic equation (6.7) may be obtained at any interior point z_* in (0, 1).

The proposed method is stable and $\boldsymbol{\Psi}\boldsymbol{\Psi}^{\mathrm{T}}=$ const. along the integration path. First it has been applied for solving (2.7), (2.9)–(2.12) using the substitutions $y_k=\Phi^{(k)}(z)$ instead of (6.1).

To integrate (6.4), (6.5) numerically, the initial conditions (6.5) are shifted from the singular point at $z_\epsilon=1-\epsilon$ (ϵ being small). In these circumstances, an additional computation procedure is needed to guarantee accuracy of the results. The basic procedure is to iterate λ until the solution λ_ϵ of the characteristic equation (6.7) is obtained with the prescribed accuracy. The same procedure has to be repeated after z_ϵ steps toward unity, with a view to convergence of the successive approximations λ_ϵ. When convergence is established with the prescribed accuracy, the last computed λ_ϵ is taken as an eigenvalue of the original problem (5.3), (2.12), with $a^0(z)$ from (5.8)–(5.12) or (5.13)–(5.15).

The successive approximations obtained as the right-hand end of the integration interval $[0, z_\epsilon]$ approaches the singular point $z=1$ are referred to as ϵ-eigenvalues. In practice, the choice of z_ϵ is limited from above by a value less than 1.0, dictated by the computer resources. Numerical experiments on a PC IBM AT/386 computer show that in order to guarantee an accuracy of 10^{-4} in a single-precision arithmetic, the integration interval cannot extend beyond 0.999.

7. Results, comparison with experiment and discussion

In figure 9 the ϵ-eigenvalues are plotted in the complex λ-plane. A rectangle in the λ-plane, bounded by $-0.5\leqslant \mathrm{Re}\{\lambda\}\leqslant 0.5$ and $3.0\leqslant \mathrm{Im}\{\lambda\}\leqslant 4.5$ was searched for eigenvalues with parameters $L_*=13.8$, $G=0.01$ and $\delta=0$, as z_ϵ tends to unity. All eigenvalues found within this rectangle are plotted in figure 9(*a*). As z_ϵ approaches unity, at values 0.986, 0.992 and 0.998 respectively, new eigenvalues appear; all ϵ-eigenvalues cluster along the imaginary axis in the left-hand half-plane. The spectrum of the original singular problem (5.3), (2.12) seems to lie along the imaginary axis or

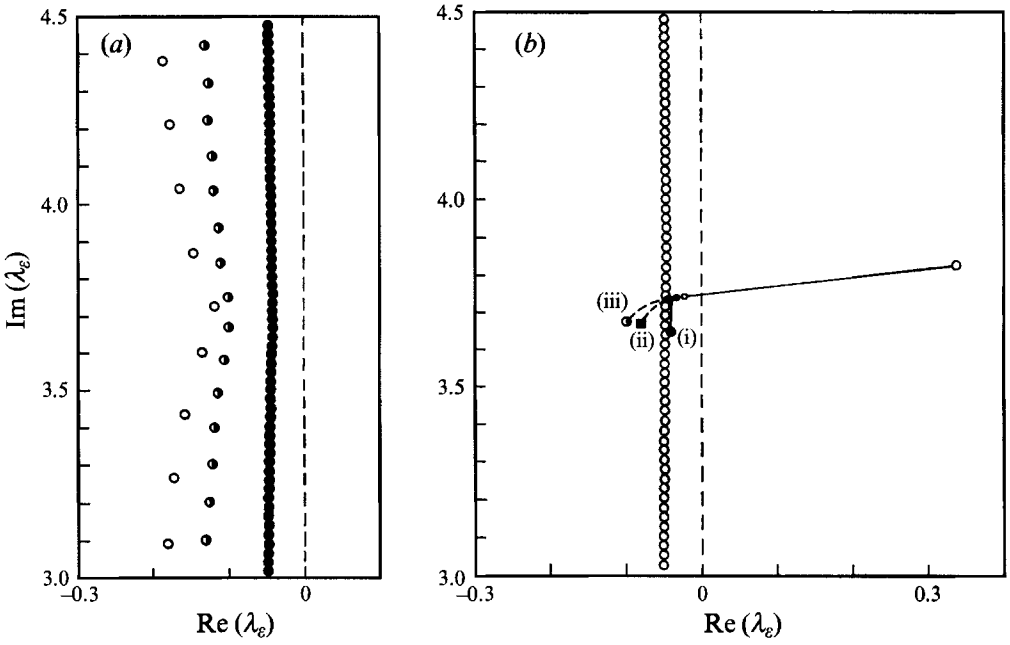

FIGURE 9. All eigenvalues lying within the interval $-0.5 < \mathrm{Re}\{\lambda\} < 0.5$ and $3.0 < \mathrm{Im}\{\lambda\} < 4.5$ at $G = 0.01$ and $\delta = 0$. (*a*) Rearrangement of ϵ-eigenvalues as z_ϵ approaches unity. $L_* = 13.80$: ○, $z_\epsilon = 0.986$; ◑, $z_\epsilon = 0.992$; ●, $z_\epsilon = 0.998$. (*b*) Grouping of ϵ-eigenvalues with increasing plate-nozzle exit distance L_*: ◑, ■, ●, $L_* = 13.80$; •, $L_* = 13.90$; ○, $L_* = 13.92$; ○, $L_* = 14.2$. Curves: (i) $z_\epsilon = 0.998$; (ii) $z_\epsilon = 0.995$; (iii) $z_\epsilon = 0.992$.

along a line parallel and close to it in the left-hand half-plane. Hence $\mathrm{Re}\{\lambda_\epsilon\} < 0$ and no instability is observed at the chosen flow parameters L_*, G and δ. The structure of the ϵ-eigenvalue spectrum shows that it is quite probably that of the singular problem (5.3), (2.12) consisting only of a continuous pattern at small values of L_* where the flow is expected to be stable. An attempt to compute the spectrum at $z_\epsilon = 0.999$ in the example of figure 9(*a*) is problematic even in double-precision arithmetic.

The grouping of the ϵ-eigenvalue spectrum as function of L_* is shown in figure 9(b). As L_* increases, all eigenvalues except one lie in the left-hand complex half-plane. At the critical value $L_* = 13.936$ an ϵ-eigenvalue appears in the right-hand half-plane, where convergence of this ϵ-eigenvalue series is clearly stated for z_ϵ above 0.992 (compare curves (i) (ii) and (iii). Hence, when searching for the critical buckling height L_{*1}, it is reasonable to set $z_\epsilon = 0.995$ and accept the corresponding ϵ-eigenvalue with the greatest real part as the first eigenvalue of the original problem (5.3), (2.12). To obtain L_{*1}, as function of the viscous, gravity and surface-tension forces, we keep track of the first eigenvalue approaching the critical value L_{*1} from above.

In figure 10 the real and imaginary parts of the first eigenvalue are plotted against L_*. It is seen that, as the latter increases, the eigenvalue appears in the upper half-plane at $L_* = 12.61$ and $L_* = 13.936$ (as in figure 9*b*) for $G = 0.02$ and $G = 0.01$ respectively. These values of L_* correspond to the onset of buckling.† Thus, the buckling height L_* decreases as the ratio of gravity to viscous forces G increases, which is in agreement with Cruickshank & Munson's (1981) experimental data.

In figure 11 the eigenfunctions corresponding to slightly supercritical viscous–gravity

† The imaginary part of the first eigenvalue $\lambda_i \neq 0$ at the onset of buckling. It obviously corresponds to the folding frequency ω_* (dimensional) at that point.

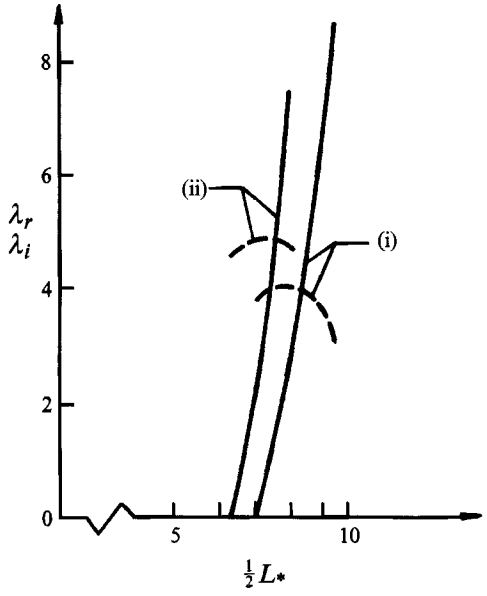

FIGURE 10. Real and imaginary parts of the first eigenvalue of λ in (5.3), (2.12). Solid curves represent λ_r, dashed ones λ_i. Curves (i) correspond to $G = 0.01$, (ii) to $G = 0.02$. For all curves $\delta = 0$.

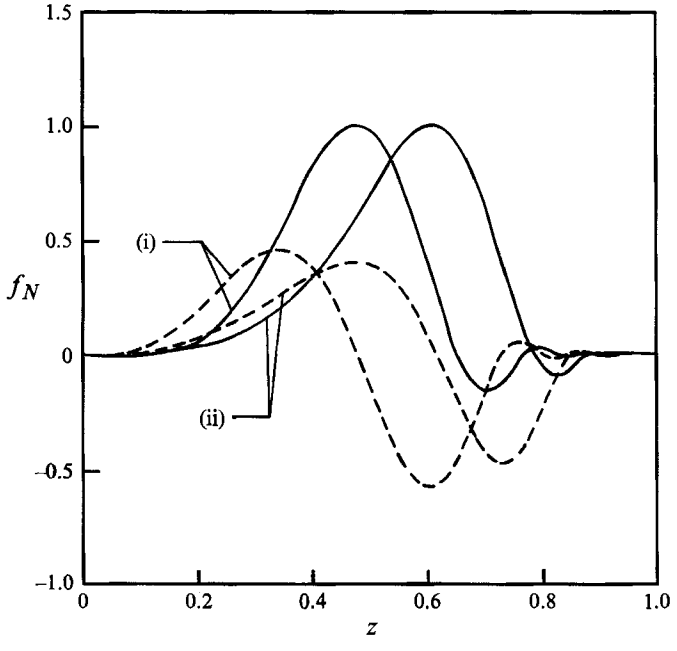

FIGURE 11. Eigenfunctions for viscous–gravity jets. Curves (i) correspond to $G = 0.01$, $L_* = 13.94$, $\beta = 1.394$ ($\lambda = 0.0047 + 3.75\mathrm{i}$); curves (ii) correspond to $G = 0.5$, $L_* = 7.365$, $\beta = 5.208$ ($\lambda = 0.0099 + 19.6744\mathrm{i}$). The solid curves show the real part of the eigenfunctions, and the dashed curves the imaginary part. The eigenfunctions are normalized by their maximum values.

jets with $\delta = 0$ are plotted, curve (i) for $\beta = 1.394 < \frac{1}{2}\pi$ (the jet in compression), and curve (ii) for $\beta = 5.208 > \frac{1}{2}\pi$ (the jet in tension high up changed to compression near the plate). It is seen that the folding motion is displaced to the plate as β grows beyond $\frac{1}{2}\pi$.

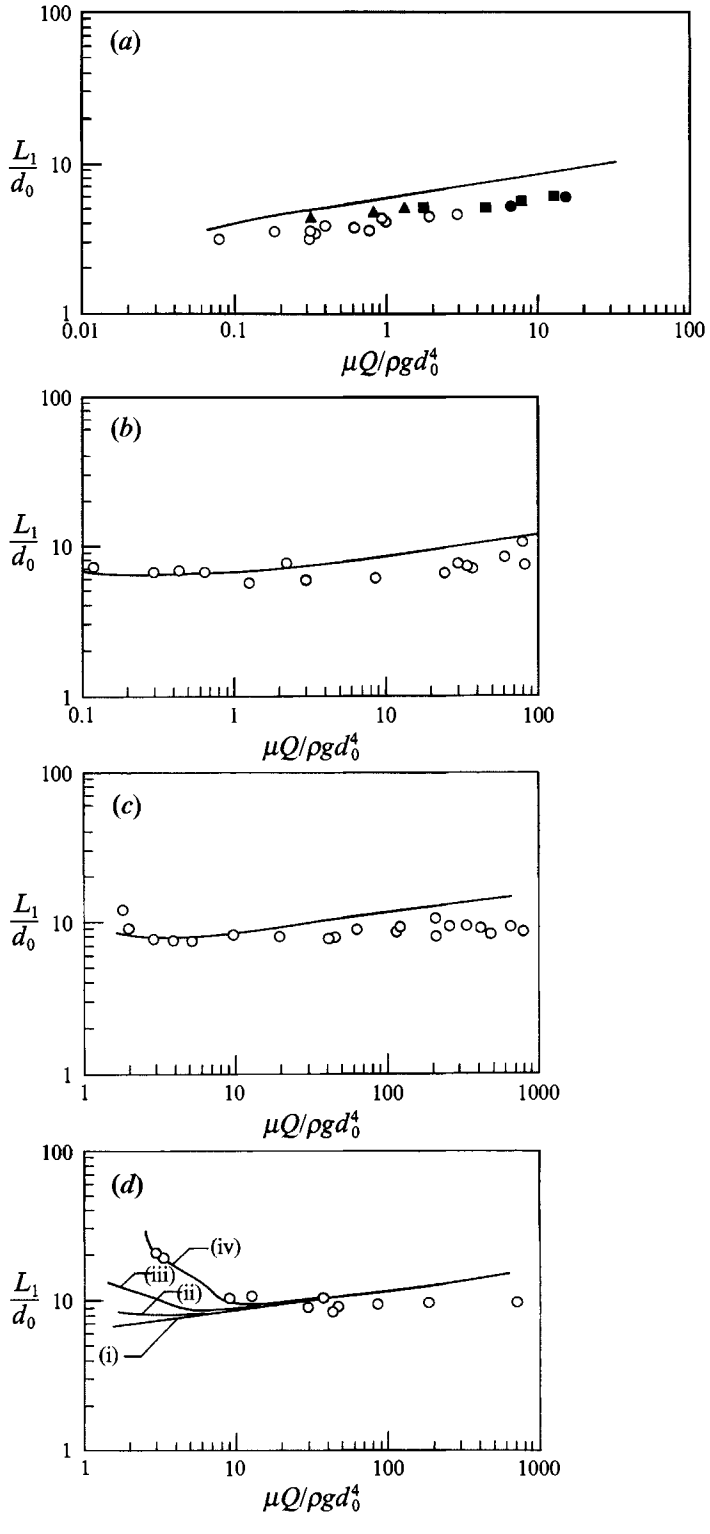

FIGURE 12. Buckling height as a function of viscous, gravity and surface-tension forces. (*a*) Low surface tension and flow rate. Curve, theoretical predictions for $\delta = 0$; ○, Cruickshank & Munson's

To compare the theoretical results with Cruickshank & Munson's (1981) and Cruickshank's (1988) experimental data, according to the Buckingham Pi theorem we need four independent non-dimensional groups, defined first in the above-mentioned papers: $\Pi_1 = \gamma/(\rho g d_0^2)$, $\Pi_2 = \mu Q/(\rho g d_0^4)$, $\Pi_3 = g d_0^3/\nu^2$, and $\Pi_4 = L/d_0$, where the nozzle diameter $d_0 = 2a_0$, the volume flow rate $Q = \frac{1}{4}\pi d_0^2 w_0^0$, and the kinematic viscosity $\nu = \mu/\rho$. (Note that in contrast to the present work, Cruickshank & Munson 1981 use the notation γ for ρg and σ for the surface tension γ.) The parameters Π_1–Π_3 may be obtained by grouping the standard Reynolds, Froude and Ohnesorge numbers.

All the other non-dimensional groups used above may be expressed in terms of Π_1–Π_3:

$$G = \frac{\pi}{96\Pi_2}, \quad L_* = 2\Pi_4, \quad \beta^2 = \frac{\pi}{24}\frac{\Pi_4^2}{\Pi_2}, \quad \delta = \pi\frac{\Pi_1\Pi_4^2}{\Pi_2}. \tag{7.1a–d}$$

The non-dimensional critical buckling height and frequency of the emerging folding, L_1/d_0 and $\bar{\omega} = \omega_* d_0/w_0^0$, measured in the experiments depend on the three non-dimensional groups Π_1–Π_3. Note also that

$$\bar{\omega} = \frac{\pi\omega_*(d_0/g)^{\frac{1}{2}}}{4\Pi_2\Pi_3^{\frac{1}{2}}} = \frac{2\lambda_i}{L_*}, \tag{7.2}$$

which means that the folding frequency $\bar{\omega}$ may be calculated by using the imaginary part of the eigenvalue λ.

Figure 12 shows the theoretical and experimental results for buckling height L_1/d_0. In figure 13 the results for the non-dimensional buckling (folding) frequency $\bar{\omega}$ are plotted. Agreement between theory and experiment is fairly good.

For the data of figure 12(*a*) the values of the ratio $\delta/6L_*$ belong approximately to the interval $(0.151 \times 10^{-2}, 0.151)$, and the values of β^2 to the interval (0.328, 32.8); for figure 12(*b*): $0.422 \times 10^{-2} \lesssim \delta/6L_* \lesssim 4.22$, and $6.42 \times 10^{-2} \lesssim \beta^2 \lesssim 64.2$; for figure 12(*c*): $1.237 \times 10^{-3} \lesssim \delta/6L_* \lesssim 1.237$, and $8.39 \times 10^{-3} \lesssim \beta^2 \lesssim 8.39$; for the experimental data and curve (iv) of figure 12(*d*): $4.64 \times 10^{-3} \lesssim \delta/6L_* \lesssim 4.64$, and

$$13.1 \times 10^{-3} \lesssim \beta^2 \lesssim 13.1.$$

For figures 12(*a*)–(*c*) β^2 is undoubtedly much larger than $\delta/6L_*$ which justifies the reduction of equation (5.5) to (5.7) when the surface tension effect on the unperturbed solution was neglected. Even in the worst case corresponding to $\gamma/\rho g d_0^2 = 1.77$ in figure 12(*d*), the values of β^2 are three times larger than the values of $\delta/6L_*$. The rather good agreement of the theoretical results with the experimental data in the worst case of figure 12(*d*) apparently shows that even in this case the effect of surface tension on the unperturbed solution of (5.5) is comparatively small and might be discarded.

Cruickshank (1988) proposed a semi-empirical model of highly viscous jet buckling (with gravity and surface tension neglected). Putting his adjustable parameter k equal to unity he obtained the critical buckling height $L_1/d_0 = 7.6634$. This value is in fairly good agreement with the experimental and theoretical data of figures 12(*b*), 12(*c*).

(1981) experimental data for $\gamma/\rho g d_0^2 = 1.15 \times 10^{-2}$. Cruickshank's (1988) experimental data: ●, $g d_0^3/\nu^2 = 2.85 \times 10^{-3}$; ■, $g d_0^3/\nu^2 = 2.57 \times 10^{-2}$; ▲, $g d_0^3/\nu^2 = 3.33 \times 10^{-4}$. (*b*) Higher surface tension: $\gamma/\rho g d_0^2 = 0.23$. Curve, theoretical results; ○, Cruickshank's (1988) experimental data. (*c*) Still higher surface tension: $\gamma/\rho g d_0^2 = 0.59$. Curve, theoretical result; ○, Cruickshank's (1988) experimental data. (*d*) Effect of surface tension on buckling height. Theoretical results: curve (i) $\gamma/\rho g d_0^2 = 0.23$ or less, (ii) 0.59, (iii) 1, (iv) 1.77. ○, Cruickshank & Munson's (1981) experimental data for $\gamma/\rho g d_0^2 = 1.77$.

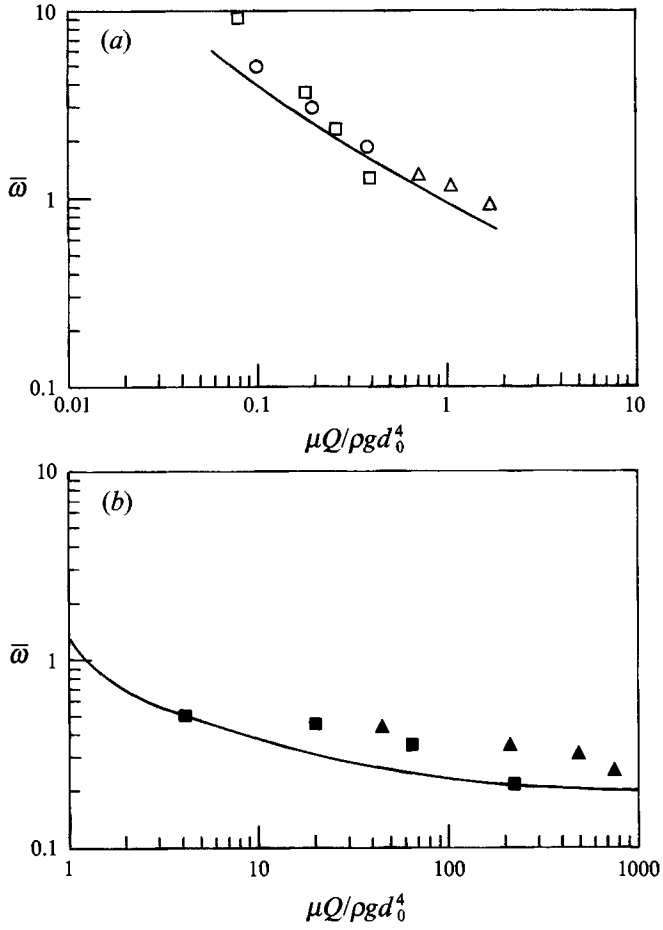

FIGURE 13. Frequency of oscillations at onset of buckling (folding). Curves: theoretical results. (*a*) Low surface tension and flow rate. Calculations with $\gamma = 0$. Cruickshank & Munson's (1981) experimental data: ○ for $\gamma/\rho g d_0^2 = 6.33 \times 10^{-3}$ and $g d_0^3/\nu^2 = 7.59 \times 10^{-2}$; △, for $\gamma/\rho g d_0^2 = 2.54 \times 10^{-2}$ and $g d_0^3/\nu^2 = 8.48 \times 10^{-2}$; □, for $\gamma/\rho g d_0^2 = 1.43 \times 10^{-2}$ and $g d_0^3/\nu^2 = 0.66$). (*b*) Higher surface tension: $\gamma/\rho g d_0^2 = 0.59$. Cruickshank & Munson's (1981) experimental data: ■, $g d_0^3/\nu^2 = 2.5 \times 10^{-3}$; ▲, $g d_0^3/\nu^2 = 8.45 \times 10^{-5}$.

However, it fails on being compared with the data of figures 12(*a*) and 12(*d*) (curve iv and the corresponding experimental data). The present theory agrees fairly well with the experimental data in figure 12(*a–d*).

Consider now the theoretical results on the behaviour of liquid jets in microgravity when $G = 0$ and $\beta = 0$. The critical buckling height is plotted in figure 14 as function of parameter $\bar{\gamma} = \gamma/6\mu w_0^0$:

$$\bar{\gamma} = \frac{\delta}{6L_*^2} = \frac{\pi}{24}(\gamma/\rho g d_0^2)/(\mu Q/\rho g d_0^4) = \frac{\pi}{24}\frac{\Pi_1}{\Pi_2}. \qquad (7.3a\text{–}c)$$

It is seen in figure 14 that as surface tension grows the critical height first decreases and then begins to increase. When $\gamma/6\mu w_0^0$ increases beyond 0.022, according to figure 14 $\delta/6L_*$ tends to unity and the critical height rapidly grows as expected (e.g. for $\bar{\gamma} = 0.031$, $\delta/6L_* = 0.86$).

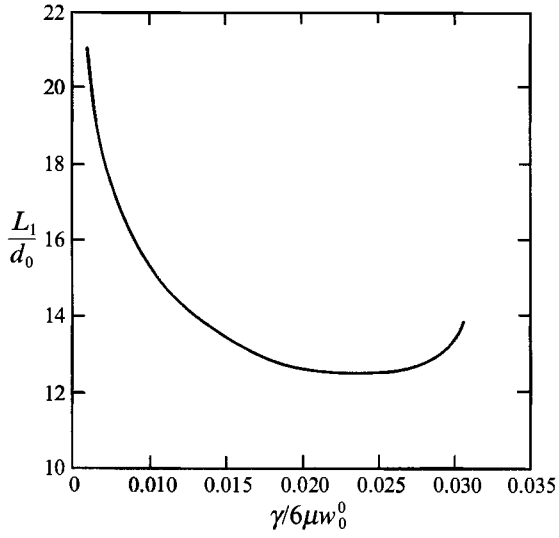

FIGURE 14. Buckling height in microgravity as function of surface-tension force.

The growth of the critical height as $\bar{\gamma}$ tends to zero looks paradoxical since in this case $\delta/6L_*$ also tends to zero and the compressive force grows (e.g. for $\delta/6L_* = 0.99$, 0.5, 0.1 and 0.01 the non-dimensional compressive force $-P$ equals -0.04, -1.24, -3.6, and -6.46, respectively).

However, considering the balance of the following force moments corresponding to the motion of a liquid in a jet in this case:

$$M_1 = \left\{3\mu A^0 \frac{\mathrm{d}w^0}{\mathrm{d}z} + \gamma\pi\left[\frac{a^0}{(1+a_{,z}^{02})^{\frac{1}{2}}} + \frac{a^{02}a_{,zz}^0}{(1+a_{,z}^{02})^{\frac{3}{2}}}\right]\right\} H, \tag{7.4a}$$

$$M_2 = -3\mu I^0\left(w^0\frac{\partial k}{\partial z} - \frac{k}{2}\frac{\mathrm{d}w^0}{\mathrm{d}z}\right) + \frac{\gamma k I^0}{a^0[1+(\mathrm{d}a^0/\mathrm{d}z)^2]^{\frac{3}{2}}}, \tag{7.4b}$$

$$M_3 = -3\mu I^0 \frac{\partial^3 H}{\partial z^2 \partial t}, \tag{7.4c}$$

we find that as $\bar{\gamma} \to 0$ the resistive moments M_2 and M_3 increase faster (due to rapid thickening of the jet) than the bending moment due to longitudinal compression M_1. This effect dominates when $\bar{\gamma}$ is smaller than 0.022, and, as a result, the critical height increases as $\bar{\gamma}$ decreases.

In contrast to this, in the region beyond $\bar{\gamma} \approx 0.022$ as $\bar{\gamma}$ decreases, the moment M_1 increases faster than M_2 and M_3 and the critical height decreases.

Note here that the steady-state model solution (2.6) possesses similar features when its stability is studied under the 'clamp' conditions (2.11) or (2.12) resulting in the emergence of the minimum in the dependence of the critical buckling height on $1/E$. This is seen in figure 8, where the critical height as well as compressive force increase as $1/E$ increases beyond its value corresponding to the minima of L_{*1}.

It is emphasized that in contrast with figure 14 (when $\bar{\gamma} < 0.022$) the results plotted in figure 12(*d*) show the growth of the critical height as surface tension increases. This means that in the viscous–gravity jets of figure 12(*d*) an increase in surface tension with fixed non-zero gravity affects, in the main, the moment M_1 which decreases with the

compressive force, whereas the critical height increases (for $\mu Q/\rho g d_0^4 = 2$–3 in figure 12(*d*): $0.01 \lesssim \bar{\gamma} \lesssim 0.116$).

8. Conclusion

The results obtained confirmed the hypothesis of G. I. Taylor (1969*a*, *b*) that buckling is due to the presence of longitudinal compression of the jet or thread and in this sense is a hydrodynamic analogue of Eulerian instability in thin elastic rods. Within the framework of the quasi-one-dimensional approach, the onset of buckling as well as the folding frequency have been quantitatively predicted.

The analysis of the present work is only a linear stability theory. Therefore, to investigate in the framework of the quasi-one-dimensional approach the interesting nonlinear behaviour found in the experiments (a regular oscillation with a reproducible amplitude and the next folding/coiling bifurcation), one needs to solve the nonlinear equations (2.1), which is worthy of future study.

B.T. and S.R. were partially supported by Bulgarian National Foundation's for Scientific Research grants No. MM5 and MM-34/91. A.L.Y. is a recipient of Guastalla Fellowship established by Fondation Rashi, Planning and Grants Committee of the Council of Higher Education, the Israel Academy of Sciences and Humanities. The work of A. L. Y. was also supported in part, by the V.P.R. Fund. The authors would like to thank Dr Katalin Balla, Computer and Automation Institute of Hungarian Academy of Sciences, for helpful discussions on the numerical method.

REFERENCES

Abramov, A. A. 1961 On the transfer of the boundary conditions for systems of ODEs. *J. Comput. Maths Math. Phys.* **1**, 542 (in Russian).

Bejan, A. 1987 Buckling flows: a new frontier in fluid mechanics. *Ann. Rev. Numer. Fluid Mech. Heat Transfer* **1**, 262.

Birkhoff, G. & Zarantonello, E. H. 1957 *Jets, Wakes and Cavities*. Academic.

Bogy, D. B. 1979 Drop formation in a circular liquid jet. *Ann. Rev. Fluid Mech.* **11**, 207.

Cruickshank, J. O. 1988 Low-Reynolds number instabilities in stagnating jet flows. *J. Fluid Mech.* **193**, 111.

Cruickshank, J. O. & Munson, B. R. 1981 Viscous fluid buckling of plane and axisymmetric jets. *J. Fluid Mech.* **113**, 221.

Cruickshank, J. O. & Munson, B. R. 1982 The viscous-gravity jet in stagnation flow. *Trans. ASME* I: *J. Fluids Engng* **104**, 360.

Debye, P. & Daen, J. 1959 Stability considerations on nonviscous jets exhibiting surface or body tension. *Phys. Fluids* **2**, 416.

Entov, V. M. & Yarin, A. L. 1984*a* The dynamics of thin liquid jets in air. *J. Fluid Mech.* **140**, 91.

Entov, V. M. & Yarin, A. L. 1984*b* Dynamics of free liquid jets and films of viscous and rheologically complex liquids. *Adv. Mech. VINITI, Fluid Mech.* **18**, 112 (in Russian).

Gurevich, M. I. 1965 *Theory of Jets of Ideal Fluids*. Academic.

Jenkins, D. R. & Barton, N. G. 1988 Computation of the free-surface shape of an inviscid jet incident on a porous wall. *IMA J. Appl. Maths* **41**, 193.

King, A. C. 1990 A note on the impact of a jet on a porous wall. *IMA J. Appl. Maths.* **45**, 139.

Matovich, M. A. & Pearson, J. R. A. 1969 Spinning a molten threadline. Steady-state isothermal viscous flows. *Ind. Engng Chem. Fundam.* **8**, 522.

Rayleigh, Lord 1879 On the capillary phenomena of jets. *Proc. R. Soc. Lond.* A **29**, 71.

Taylor, G. I. 1969*a* Instability of jets, threads and sheets of viscous fluid. *Proc. 12th Intl Congr. Appl. Mech., Stanford, 1968*, p. 382.

TAYLOR, G. I. 1969*b* Electrically driven jets. *Proc. R. Soc. Lond.* A **313**, 453.

VASSALLO, P. & ASHGRIZ, N. 1991 Satellite formation and merging in liquid jet breakup. *Proc. R. Soc. Lond.* A **433**, 269.

WEBER, C. 1931 Zum Zerfall eines Fluessigkeitsstrahles. *Z. Angew. Math. Mech.* **11**, 136.